Computational design of flexible functional two-dimensional materials

Ji Soo Nam

Department of Energy Engineering
(Energy Engineering)

Graduate School of UNIST

Computational design of flexible functional two-dimensional materials

A thesis/dissertation
submitted to the Graduate School of UNIST
in partial fulfillment of the
requirements for the degree of
Master of Science

Ji Soo Nam

12/14/2018

Approved by

Advisor
Jun Hee Lee

Computational design of flexible functional two-dimensional materials

Ji-Soo Nam

This certifies that the thesis/dissertation of Ji-Soo Nam is approved.

12/14/2018

signature

Advisor: Jun Hee Lee

signature

typed name: Geun Sik Lee

signature

typed name: Jung Woo Yoo

I. Abstract

Two-dimensional materials have received great attention after the discovery of graphene. It has not only outstanding electrical, thermal properties but also many advantages for device application such as flexibility.

Here, we report that first, polar distortion can occur only by the symmetry breaking of a very simple collinear spin ordering in a low dimensional system lacking translation. Second, multistate material can be designed by giving intrinsic structural anisotropy to the single state ferroelectric material.

For the first work, we have shown that in the materials with an odd number of magnetic layers, and with strong covalent bonds of constituent atoms, such as FGT, spin-phonon coupling results in the formation of a giant polar distortion(~0.2Å) in various antiferromagnetic meta states where translation cannot be compensated by using Fe_3GeTe_2 monolayer as a model system. This order is much larger than the normal spin origin polar distortion (~ 0.01Å)[1] and even larger than the polar distortion of conventional ferroelectric materials such as BaTiO3 and BiFeO3[2, 3]. It is expected that not only FGT but also materials with strong bonding between atoms and low-dimensional characteristics of two-dimension and odd layers can exhibit a huge polar distortion due to change of magnetic state. The formation of a large ferroelectric by simple collinear spin ordering in a low dimensional system will open a new chapter in the discovery and application of new states of low dimensional materials as a general method applied to all two-dimensional materials[4].

For the second work, we mixed GeTe and SnTe which are experimentally confirmed as ferroelectric material[5, 6] to make the structural anisotropic material. we used $GeSnTe_2$ that imaginary material which have in-plane structural anisotropy as a model system. For this anisotropic mixing structure, a-directional polarization and b-directional polarization of $GeSnTe_2$ is not the same anymore. This two different polarization values and barrier energies of a-directional and b-directional polarized phase makes the multistate application possible.

Contents

List of figures

Figure 12. Barrioer energy of direct path from -Pa,-Pb phase to +Pa,+Pb phase for polarization switching obtained from NEB calculation.

Figure 13. Barrioer energy of rotational path from -Pb phase to +Pa phase to +Pb phase for polarization switching obtained from NEB calculation.

List of tables

II. Computation method

2.1 Density Functional Theory

All the materials are made up of atoms, which consist of a large number of electrons and nuclei. The reason for the different properties of materials is that the bonding states of the atoms arranged inside are different and the more basic reason is that the surrounding electrons that mediate the bonding of atoms have different characteristics. Therefore, to understand the properties of a material, it is necessary to understand the behaviors of electrons and nuclei in the material. In principle, we can describe all the behaviors of electrons and nuclei using the Schrodinger equation and obtain the properties of the system by solving the Schrodinger equation. However, it is practically impossible to solve the Schrodinger equation of a system containing many electrons and nuclei. To solve this problem, several approximations were introduced. The first one is Born-Oppenheimer approximation. It is assumed that the nucleus which is several thousand times heavier than an electron is fixed thereby the Hamiltonian is expressed as the movement of electrons in the electric field by the nucleus.

$$\boldsymbol{H = \frac{h^2}{2m}\sum_{i=1}^{N}\nabla_i^2 + \sum_{i=1}^{N}V(r_i) + \sum_{i=1}^{N}\sum_{j<i}U(r_i, r_j)}$$

In the Hamiltonian, the first, second and third terms describe the kinetic energy of each electron, the interaction energy between each electron and the collection of atomic nuclei, and the interaction energy between different electrons, respectively. However, we still have difficulties solving the equation exactly in many electrons system because the individual electron wave function cannot be found without simultaneously considering the individual electron wave functions associated with all the other electrons.

Density functional theory is simply a theory that the ground state total energy and any physical properties of a system with many electrons can be obtained by knowing only ground state electron density without considering all the wave functions of each electrons.

2.1.1 The Hohenberg-Kohn Theorems

Hohenberg-Kohn proved that

I. The external potential (V_{ext}) is a unique functional of the electron density (n(r)).
II. A universal functional for the energy E[n] can be defined in terms of the density. The exact ground state is the global minimum value of this functional, and the density that minimizes the total energy is the exact ground state density.

Since the wavefunction and Hamiltonian is uniquely determined by external potential, the ground state total energy and all other the ground state properties are determined by electron density. We can write the total energy

$$\mathrm{E[n(r)]} = \int V_{ext}(r)n(r)dr + T[n(r)] + E_{ee}[n(r)] = \int V_{ext}(r)n(r)dr + F[n(r)]$$

Because the treatment for kinetic and electron-electron repulsion energies are independent of systems. We can obtain the exact electron density using variational principle which is satisfy the second theorem. But the problem was that the explicit form of F[n(r)] is not exactly known.

2.1.2 The Kohn-Sham equation

To solve above problem, Kohn and Sham proposed fictitious system that non-interacting electrons moving in effective Kohn-Sham potential. They solved Schrödinger equation for one-electron and combined one-electron wavefunctions (molecular orbitals) to obtain approximate wavefunction for all electrons. by doing this, theoretically we can obtain exact density of interacting electrons. The Kohn-Sham equation is

$$\left[\frac{h^2}{2m}\nabla^2 + V(r) + V_H + V_{XC}\right]\psi_i(r) = \varepsilon_i\psi_i(r), \qquad V_{XC} = \frac{\delta E_{XC}}{\delta n(r)}$$

The equation including three different potential. $V(r)$ is external potential, V_H is coulomb potential and V_{XC} defines exchange and correlation contributions to the single-electron equation. To solve this equation, the exchange-correlation term must be approximated.

III. Design of low dimensional multiferroics.

3.1 Introduction

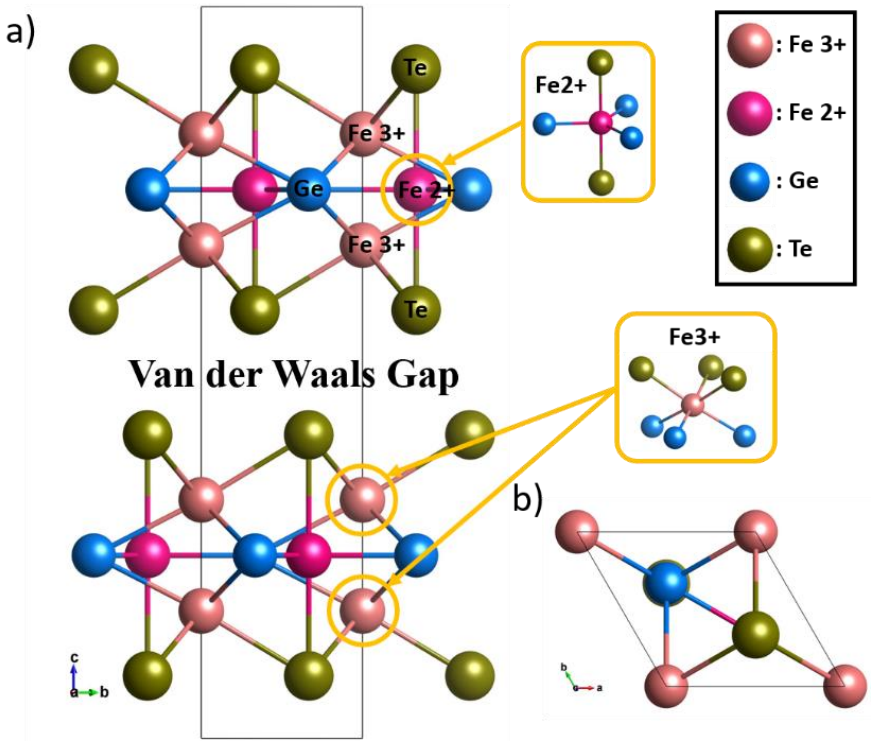

Figure 1 | Crystal structure of bulk Fe_3GeTe. a) and b) shows side view and top view respectively.

After Maxwell established the relationship between the electric field and the magnetic field in 1865[7], it was first demonstrated experimentally with Cr_2O_3 that the electric field can control the magnetic property[8]. Following the discovery of Cr_2O_3, studies on ferroelectric originating from spin have been continued. Among them, the most widely known mechanism is that polarization is induced by inverse DM interaction in a noncollinear spin structure by magnetic frustration[1, 9]. The polar distortion induced by the collinear spin structure is rare, most of which is induced by double exchange in complex E-type antiferromagnetic ordering[10, 11]. However, we have found that polar distortion can occurs only by the symmetry breaking of a very simple collinear spin ordering in a low dimensional system lacking translation.

We chose Fe_3GeTe_2 as a model system. It is a highlighted example of ferromagnetic metallic van-der Waals material. As Figure 1 shows, each FGT unit layer contain 3 iron layers. Top and bottom iron has the same Wyckoff position and the same oxidation number while the middle one has different Wyckoff position and different oxidation number[12]. Since it has Van der Waals layered structure, the bonding

between layers is weak and it does not have dangling bond on the surface of layer. That makes exfoliation easier. Fe_3GeTe_2 possesses unusually strong magnetic interaction proven by the one of the highest ferromagnetic critical temperature (> 200 K)[13, 14] among van der Waals materials. In addition, FGT composes of three iron layers with other ligand ions with a plenty of space between tri-layers Therefore, we first speculated that if bonds between Fe ions could be broken (recovered) by antiparallel (parallel) spin configuration, Fe ions would be largely displaced perpendicular to the layers.

The formation of a large ferroelectric by simple collinear spin ordering in a low dimensional system will open a new chapter in the discovery and application of new states of low dimensional materials as a general method applied to all two-dimensional materials.

3.2 Computational details

First principles calculations were performed using density-functional theory (DFT) within the generalized gradient approximation GGA+U method with Perdew-Becke-Erzernhof parametrization as implemented in the Vienna ab initio simulation package (VASP 5.4.1)[15-18]. We use the Dudarev[19] implementation with on-site Coulomb interaction U = 3.0 eV for Fe to treat the localized 3d electron states. The projector augmented wave (PAW) potentials[20, 21] explicitly include 14 valence electrons for Fe ($3p^6\ 3d^6\ 4s^2$), 14 for Ge ($3d^{10}\ 4s^2\ 4p^2$), 6 for Te ($5s^2\ 5p^4$). Exchange constant calculation were computed in supercell with 1×2×1 primitive cell and 2×2×1 supercell used for various spin ordering structure calculations. A plane wave basis set with a cutoff energy of 500 eV is used. The k-point sampling uses the Gamma centered Monkhorst-Pack scheme[22] and employs a 18×18×1 and a 9×9×1 mesh for structure optimization of the primitive cell and the 2×2×1 supercell of Fe_3GeTe_2 monolayer. The atomic positions were optimized until the interatomic forces are smaller than 1meVÅ^{-1}. For exchange constant J calculation, we used energy mapping analysis[23] with general spin Hamiltonian for localized spin.

$$\mathrm{H} = \sum_{i,j} -J_{ij} S_i \cdot S_j$$

$$E_1 = E_0 + E_{other} + J_{12}S^2 + K_1S + K_2S$$
$$E_2 = E_0 + E_{other} - J_{12}S^2 + K_1S - K_2S$$
$$E_3 = E_0 + E_{other} - J_{12}S^2 - K_1S + K_2S$$
$$E_4 = E_0 + E_{other} + J_{12}S^2 - K_1S - K_2S$$

$$J_{12} = \frac{E_1 + E_4 - E_2 - E_3}{4S^2}$$

3.3 Result and discussion

3.3.1 Spin induced ferroelectricity in FGT monolayer

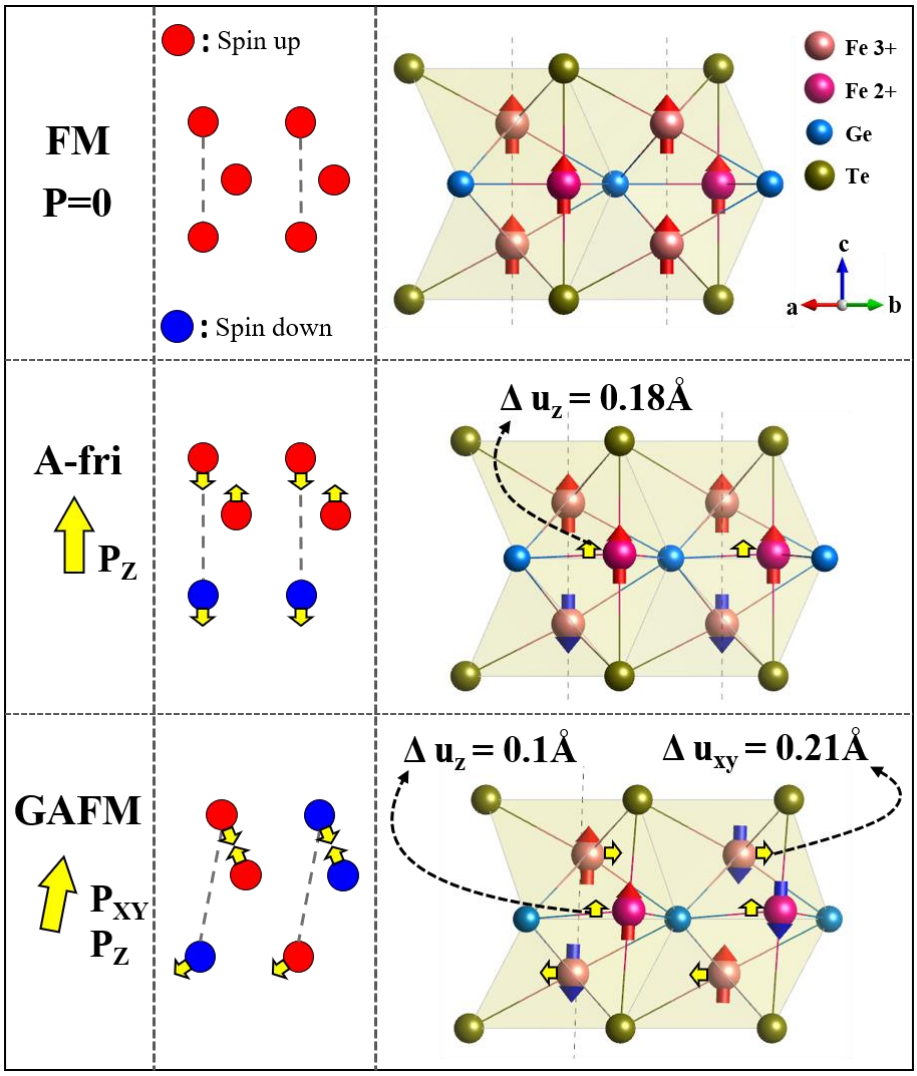

Figure 2 | Schematics of atomic displacements depending on magnetic ordering in 3 layers hexagonal system and DFT calculated atomic structure of Fe_3GeTe_2

Our expectation was that symmetry breaking of spin ordering may induce structural polar displacement in the low dimensional magnetic materials. To confirm the idea, we used FGT mono layer as a practical example. Figure 2 shows Schematics of atomic displacements depending on magnetic ordering in three layers hexagonal system and DFT calculated atomic structure of Fe_3GeTe_2 monolayer. Red circle represents magnetic ion with up spin and blue circle represents magnetic ion with down spin. Firstly, ferromagnetic spin ordering doesn't break any symmetry element of original paramagnetic

structure. Calculated FGT structure also shows that ferromagnetic ordering conserves its paramagnetic original space group of 187($P\bar{6}m2$)[24] which has point group of D_{3h}.

For the next, A-type ferrimagnetic spin ordering which means top and bottom iron sub lattice has A-type AFM spin structure and middle iron sub lattice has ferromagnetic spin ordering, breaks σ_h (horizontal mirror symmetry). Therefore, we expected that the spin structure would induce z directional polar displacement. I will call this A-type ferrimagnetic structure just A-fri. We relaxed FGT structure with A-fri spin ordering and found that about 0.18 angstrom of z directional polar displacement occurred. the space group of FGT_A-fri structure became 156(P_{3m1}) and the point group reduced to C3v which is polar since horizontal mirror symmetry was broken by spin ordering.

The last one is G-type antiferromagnetic spin ordering. Strictly speaking, it is not G-type AFM. It cannot have G-type AFM spin structure because it has trigonal lattice system. But I will just call it G-AFM since if we see the top and bottom iron sublattice, it looks like G-type AFM in some sense. Figure 2 will help understanding spin ordering of FGT. We expected appearance of in-place and out of plane polar displacement since G-AFM spin ordering breaks two σ_v (vertical mirror symmetry) as well as σ_h. After relaxation of FGT structure with G-AFM spin ordering, the relaxed structure showed about 0.1 angstrom of z directional polar displacement and 0.2 angstrom of xy directional polar displacement. the symmetry of FGT_G-AFM relaxed structure reduced very much, the space group became 8(Cs-3) and point group became Cm since two σ_v and σ_h were broken by spin ordering. Those results are consistent with our expectation[24].

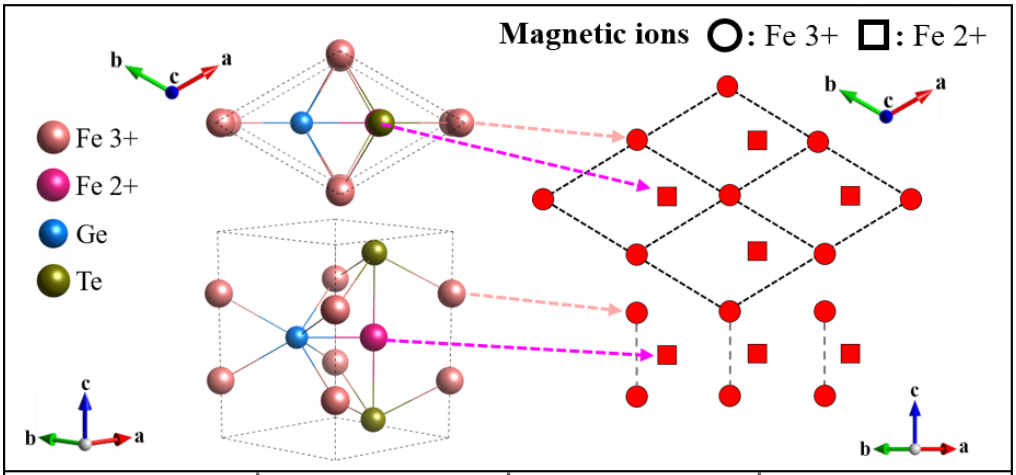

FM	G-AFM	G-Ferri	C-AFM1
ΔE = 0meV	**ΔE = 25meV**	ΔE = 29meV	ΔE = 29meV
A-AFM	A-Ferri	C-AFM2	C-Ferri
ΔE = 57meV	**ΔE = 68meV**	ΔE = 77meV	ΔE = 59meV

Figure 3 | Skimatics of various spin ordering and the total energy difference of the phases compare to ferromagnetic groud state energy.

We also tried many other spin orderings on FGT system in addition to the above three and confirmed that the symmetries of atomic displacements were depending on the symmetries of spin ordering. Atomic displacements appeared for all the spin ordered structures different from ferromagnetic ground state structure. But nonpolar spin ordering induced only nonpolar atomic displacements. For example, in case of fri-centro spin ordering which has ferromagnetic relation between Top iron and Bottom iron and antiferromagnetic relation between Top iron and Middle iron, it also shows atomic displacement after relaxation of the structure. But the displacement is nonpolar and only the thickness of the layer increase. Figure 3 shows the various spin ordering what I have tried and their energy difference from ferromagnetic ground state structure. As is well known, Ferromagnetic structure has lowest energy and second one is G-AFM structure. The energy difference is only 25meV/(Fe ion).

3.3.2 Origin of the polar displacements

3.3.2.1 Microscopic origin

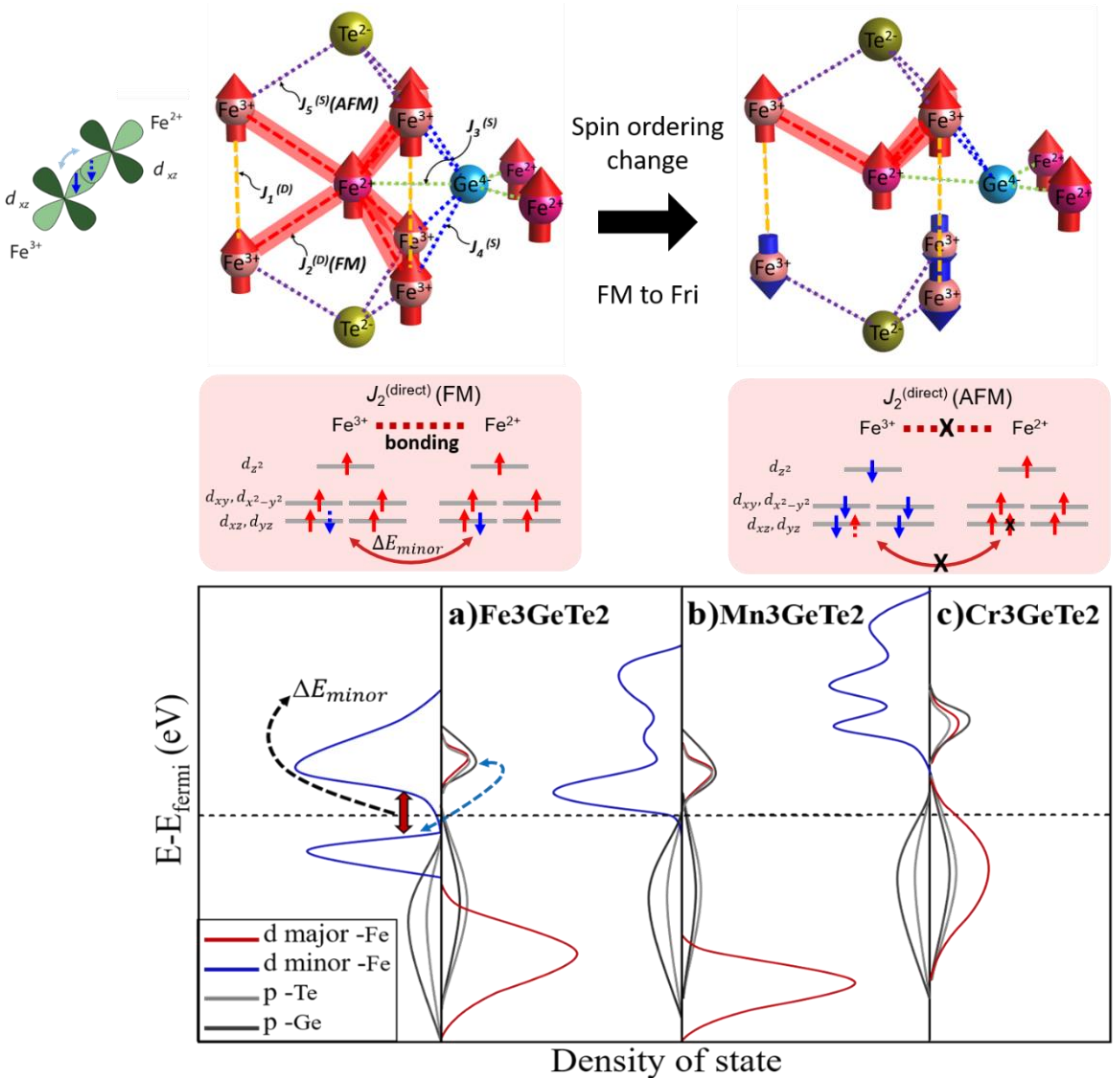

Figure 4 | The origin of the strong coupling between polar distortion and spin structures. Top figures shows that exchange interaction of FM and A-fri and bottom figure shows simplized density of state of Fe_3GeTe_2, Mn_3GeTe_2 and Cr_3GeTe_2.

We confirmed our prediction of the emergence of polar displacement through symmetry breaking induced by spin ordering. From now on, I will explain the microscopic origin of the movement of each atom and this huge displacement about 0.2 angstrom. It is extremely large value as a spin driven

displacement. If we compare this displacement to that of BiFeO3, which is well known ferroelectric materials, the polar displacement is about 10 times of BiFeO3[25].

To understand this phenomenon, Firstly, we must understand exchange interaction of FGT. In Figure 3, A-fri spin ordering is used as a simplest spin ordering which induce polar displacement to explain the origin. The red arrows penetrate Fe ions represent majority spin and the blue arrows penetrate Fe ions represent minority spin. The dash lines between irons represents direct exchange paths which connect two magnetic ions directly and the dotted lines represent super exchange paths which connect two magnetic ions through mediated ion. All the different color of lines represents different exchange interactions. As the figure shows, FGT has a lot of different exchange paths between magnetic Fe ions. Among them, the strongest exchange interaction is a double exchange interaction. The interaction between top iron and middle iron and between bottom iron and middle iron which denoted by thick red lines. Because the oxidation number of middle iron is assumed as 2+ and that of top and bottom iron is assumed as 3+, middle iron has d^6 electronic structure and top and bottom iron has d^5 electronic structure[12]. To make the electron hoping from the d^6 state of middle iron to d^5 state of top and bottom iron possible, the double exchange interaction strongly favors ferromagnetic relation between them. In case of A-fri spin ordering, the double exchange path between middle iron and bottom iron is broken since electron hopping is prohibited by the Pauli exclusion principle. Figure 3 shows schematics of that and orbital picture. As a result, to relieve the penalty of anti-parallel double exchange interaction, structural distortion occurs. the distance between middle iron and bottom iron is increased and the distance between top iron and middle iron is decreased.

Table 1 shows the result. After relaxation with A-fri spin ordering, Fe-top moves about 0.075 Å to -z direction, Fe-bottom moves 0.113 Å to -z direction and Fe-middle moves about 0.125 Å to z direction. It is consistent with above idea.

As I mentioned before, the displacement induced by spin ordering is very huge in FGT system compare to typical spin driven ferroelectric materials. Firstly, dimensionality can be responsible for the huge displacement because a plenty of space boosts up atomic displacement in low dimension. But it cannot explain huge force that emerge from change of spin ordering without lattice relaxation. To understand the reason of huge force, I investigated the effect of transition metal in FGT system. I substitute Fe to other transition metals such as Cr and Mn and checked the force difference between ferromagnetic and A-fri state with ferromagnetic relaxed structure. The result is that Mn_3GeTe_2 shows very small force and Cr_3GeTe_2 shows force about half of Fe_3GeTe_2. By analyzing their density of state, firstly, we found out that the energy levels of atoms are similar so orbital hybridization is large in FGT system. Secondly, FGT has a lot of spin minority d state above and below the fermi level and the gap between them is small while Mn_3GeTe_2 doesn't have d states that close enough to interact each other

for neither majority and minority part of dos. For Cr_3GeTe_2 case, it has some spin majority d states that can interact each other. These results tell us that d states near above and below the fermi level and the small gap between them contribute to strong interaction between middle iron and top or bottom irons and that makes J_2 very strong.

		FM	A-fri	Displacement(Å)
	thickness	5.386	5.500	0.114
Position (Cartesian)	Fe-Top	5.5143	5.6169	-0.075
	Fe-Bottom	2.7043	2.7689	-0.113
	Fe-Middle	4.1093	4.4119	0.125
	Ge	4.1093	4.3068	0.020
	Te1	6.8022	7.0580	0.078
	Te2	1.4162	1.5582	-0.036
magnetic moment	Fe1	3.109	3.206	
	Fe2	3.109	-3.252	
	Fe3	2.690	2.680	
	$E-E_{FM}$ (eV/unitcell)	0.00	0.20	
	$E-E_{FM}$ (meV/Fe atom)	0.00	67.60	

Table 1 | Atomic displacement and magnetization of A-fri phase compare to FM phase. It shows both polar displacement and non-polar displacement.

In addition, I calculated exchange interaction constant J_1 between top iron and bottom iron, J_2 between top iron and middle iron and J_5 between top iron and top iron(in-plane). Each exchange constant is affected by many different exchange paths. For example, J_1 is affected by at least two exchange paths. One is direct exchange and the other one is super-exchange mediated by Germanium ion. The direct path was thought to favor antiferromagnetic relation but 7.7meV of J_1 value means that it weakly favors ferromagnetic relation. Therefore, I think the super-exchange path mediated by Germanium may favor ferromagnetic relation and the competition of both paths makes the J_1 smaller compare to J_2 (35.9meV).

In-plane exchange interaction is more complicated because it has triangular lattice and so many different paths exist. Since it is too difficult to consider all the interaction, I will just discuss only some possible orbital picture. figure 4, thick purple line represents one of super-exchange path between top

iron and top iron that mediated by Te ion and thick green line represents one of super-exchange path between middle iron and middle iron that mediated by Ge ion. The orbital picture of figure 4 is applicable for both paths. It shows that the super-exchange path favors antiferromagnetic relation because two electrons must have different spins to share the same p orbital based on Pauli exclusion principle. Besides, many super-exchange paths exist. Super-exchange path generally favors ferromagnetic relation or antiferromagnetic relation depending on interacting orbital and angle between the path. The calculated J_5 value is -2.2meV and it means that sum of the effects of all the exchange interactions between top iron and top iron very weakly favors antiferromagnetic relation. The competition of many different exchange interaction can be responsible for the such a small value.

In-plane exchange constant J_5 which favors antiferromagnetic relation explains that G-AFM structure is energetically more stable than A-fri structure.

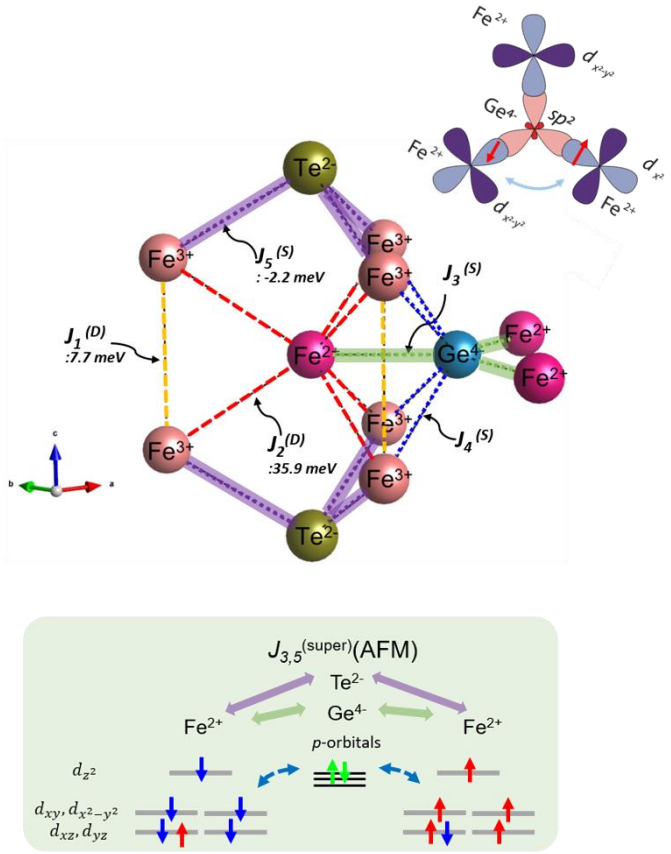

Figure 5 | The crystal structure of Fe_3GeTe_2 with multiple exchange paths and electronic state of atoms. The indirect exchange path via the intermediate ligands, Ge^{4-} and Te^{2-}, denoted as J_3 and J_5. The electronic configuration figure shows that this exchange interaction favors the antiferromagnetic relation due to superexchange mechanism.

3.3.2.2 Macroscopic origin

Here we will confirm the idea that symmetry breaking of spin ordering may induce structural polar displacement in the low dimensional magnetic materials more clearly by using group theoretical analysis. Firstly, we will start with the simplest A-fri spin ordering.

Fri	f	a	c	p_z	E
$\widehat{\sigma_h}$	1	$\bar{1}$	1	$\bar{1}$	1
$\hat{T}$	$\bar{1}$	$\bar{1}$	$\bar{1}$	1	1
basis	$\sigma_1\begin{pmatrix}1\\0\\1\end{pmatrix}$	$\sigma_1\begin{pmatrix}1\\0\\\bar{1}\end{pmatrix}$	$\sigma_2\begin{pmatrix}0\\1\\0\end{pmatrix}$	u_{polar_z}	$u_{nonpolar}$

Table 2 | Order parameters and symmetry considering character table for A-fri phase. the first, second and third row of basis functions that related to spin ordering represent sign of spin of top, middle and bottom iron respectively.

f : ferromagnetic relation between top iron and bottom iron
a : antiferromagnetic relation between top iron and bottom iron
c : ferromagnetic relation between middle irons
P_z: z-directional polar displacement
ε : z-directional non-polar displacement (strain)

In Table 2, the first row represents order parameters of A-Fri structure and the first column represent symmetry operations. Since A-fri break horizontal mirror plane and spin breaks time reversal symmetry, the two symmetry operations appear on the table. The table shows that whether each order parameter is invariant for the symmetry operations or not. For example, the characters of f, a and c order parameters are all -1 for time reversal symmetry since those three order parameters are related spin and spin breaks time reversal symmetry. Also, horizontal mirror symmetry is broken for a and P_z order parameters.

Now we can write down landau free energy equation. Only these below terms are group theoretically allowed coupling

$$G = G(PM,PE) + \sum_{i=1}^{5} \alpha_i \dot{O}_i^2 + \beta \cdot f \cdot c + C_{31}(a \cdot c \cdot p_z) + C_{32}(f \cdot a \cdot p_z) + \varepsilon \sum_{i=1}^{5} C'_{3i} \cdot \dot{O}_i^2 + C_{33}(f \cdot c \cdot \varepsilon)$$

$$\text{Force} = F = -\left.\frac{\partial G}{\partial P}\right|_{P=0} \rightarrow F = C_{31} \cdot a \cdot c + C_{32} \cdot f \cdot a$$

And the dipolar force can be obtained by differentiating free energy with polarization. By using this equation, we can finally obtain the force difference between ferromagnetic spin ordering and ferrimagnetic spin ordering.

	f	a	c
FM	1	0	1
A − fri	0	1	1

Table 3 | The values of spin related order parameters for ferromagnetic and A-fri spin ordering.

As table 3 shows, f and a order parameters of ferromagnetic spin ordering is 1 and 0 and that of A-fri spin ordering is 0 and 1. c order parameter is 1 for both case. If we assign the values into above equation, we can get below result.

$$\Delta F = F(A - fri) - F(FM) = C_{31} \cdot a \cdot c - 0 = C_{31} \cdot a \cdot c$$

The result clearly shows that the emergence of dipolar force is related to only the coupling of antiferromagnetic relation between top iron and bottom iron and ferromagnetic middle iron.

For the next, we will apply group theory to the more complicated spin ordering G-AFM. For this case, we must consider in-plane spin ordering as well.

	Ff	Fa	Af	AA	CF	CA	p_z	p_{xy}	E
$\widehat{\sigma_h}$	1	$\bar{1}$	1	$\bar{1}$	1	1	$\bar{1}$	1	1
$\hat{T}$	$\bar{1}$	$\bar{1}$	$\bar{1}$	$\bar{1}$	$\bar{1}$	$\bar{1}$	1	1	1
$\widehat{\sigma_{v1}}$	1	1	$\bar{1}$	$\bar{1}$	1	$\bar{1}$	1	$\bar{1}$	1
$\widehat{\sigma_{v2}}$	1	1	$\bar{1}$	$\bar{1}$	1	$\bar{1}$	1	$\bar{1}$	1
basis	$\sigma_1\begin{pmatrix}1\\1\\0\\0\\1\\1\end{pmatrix}$	$\sigma_2\begin{pmatrix}1\\1\\0\\0\\-1\\-1\end{pmatrix}$	$\sigma_3\begin{pmatrix}1\\-1\\0\\0\\1\\-1\end{pmatrix}$	$\sigma_4\begin{pmatrix}1\\-1\\0\\0\\-1\\1\end{pmatrix}$	$\sigma_5\begin{pmatrix}0\\0\\1\\1\\0\\0\end{pmatrix}$	$\sigma_6\begin{pmatrix}0\\0\\1\\-1\\0\\0\end{pmatrix}$	u_{polar_Z}	u_{polar_xy}	$u_{nonpolar}$

Table 4 | Order parameters and symmetry considering character table for G-AFM spin ordering. The first, third and fifth row of basis functions that related to spin ordering represent signs of spin of top, middle and bottom iron respectively. The second, fourth and sixth row also represent signs of spin of top, middle and bottom iron respectively but they are different from previous ones. They are next to the previous one. Therefore the new order parameters can represent in-plane AFM spin ordering as well as out of plane AFM spin ordering.

D3h	E	2C3	3C2	σ_h	$2S_3$	$3\sigma_v$		
A_1'	1	1	1	1	1	1		x^2+y^2, z^2
A_2'	1	1	- 1	1	1	- 1	Rz	
E′	2	- 1	0	2	- 1	0	(x,y)	$x^2 - y^2$, xy
A_1''	1	1	1	- 1	- 1	- 1		
A_2''	1	1	- 1	- 1	- 1	1	z	
E″	2	- 1	0	- 2	1	0	(Rx,Ry)	(xz,yz)

Table 5 | Character table for D3h point group.

	E	2C3	3C2	σ_h	$2S_3$	$3\sigma_v$		$\hat{T}$
AA	2	- 1	0	- 2	1	0	E''	-1
CA	2	- 1	0	2	- 1	0	E'	-1
Pxy	2	- 1	0	2	- 1	0	E'	1
Pz	1	1	1	- 1	- 1	- 1	A_2''	1

Table 6 | Characters of non-zero order parameters considering symmetry operation of D3h point group.

	Ff	Fa	Af	Aa	CF	CA
FM	1	0	0	0	1	0
GAFM	0	0	0	1	0	1

Table 7 | The values of spin related order parameters for ferromagnetic and G-AFM spin ordering.

For FM, force is zero and non-zero order parameter for GAFM is only AA, CA, P_{xy}, P_z and ε. But we don't consider ε since it is totally symmetric.

We have to consider that AA, CA, P_{xy} is doubly degenerated.

We can match up the order parameters with the irreducible representation of D_{3h} which is point group of PM FGT. AA, CA, P_{xy}, P_z are match with E'', E', E', A_2'' respectively. Since AA and CA has minus sign for time-reversal symmetry, allowed combination of them should be even order product of AA and CA. Therefore, if we consider only quadratic order for magnetic order parameter, there are only these 3 possibilities $(AA)^2$, $(CA)^2$, (AA)*(CA). And the symmetric representation is $E'' \times E''$, $E' \times E'$ and $E' \times E''$

and each of them can be decomposed in this way

$$E'' \times E'' = 2A_1' + 2A_2' + 2E'$$
$$E' \times E' = 2A_1' + 2A_2' + 2E'$$
$$E' \times E'' = 2A_1'' + 2A_2'' + 2E''$$

Therefore, symmetrically allowed terms for AA, CA, P_{xy}, P_z are

(AA)*(AA)*(P_{xy}), (CA)*(CA)*(P_{xy}) and (CA)*(AA)*(P_z)

Then the dipolar force for P_z is proportional to the coefficient of (CA)*(AA) and it is consistent with Fri case. And the dipolar force for P_{xy} are arise from both of (AA)*(AA) and (CA)*(CA) coupling.

3.3.3 Achieving ferroelectric phase by strain engineering

Even though we found out that spin ordering can induce polar displacement, there still is a problem using a ferroelectric phase of FGT. Originally the ground state of FGT is ferromagnetic non-polar phase and we already showed that strong double exchange interaction between Fe^{2+} and Fe^{3+} stabilize ferromagnetic phase. It means that when we change the spin ordering, it becomes energetically unstable by the ferromagnetic exchange interaction. Since atomic displacements relive the effect, the energy differences between ferromagnetic structure and other spin ordering structures are reduced. As figure 2 shows, G-AFM structure has the lowest energy close to ferromagnetic structure energy among the spin ordering that induce polar displacement. The energy difference between them is about 25meV/Fe ion. This value is small enough to overcome with some engineering.

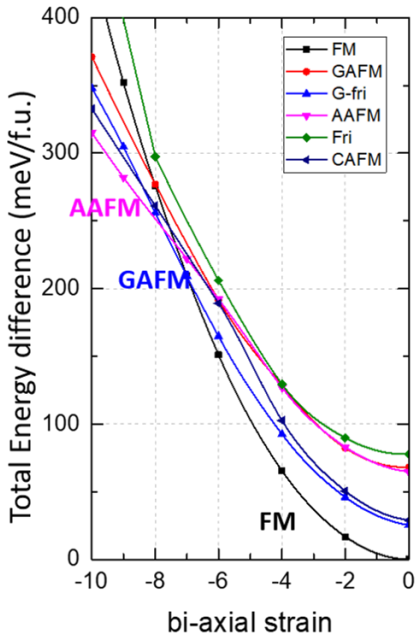

Figure 6 | Total energy of various spin induced structures where unstrained ferromagnetic ground state energy is set to zero. Calculation were performed at integer strain and interpolated.

We used strain engineering to stabilize the G-AFM phase. The reasons of that are first, the 2d material is much more flexible than the 3d material and second, the exchange constant J that determining the magnetic state is changed depending on distance and angle between ions and we can modulate the distance and angle using strain engineering. Figure 6 is a graph that shows total energy of various spin ordering structure as bi-axial compressive strain is applied where unstrained ferromagnetic ground state energy is set to zero. Without strain, it is clear that all other spin ordered structure has higher energy

than ferromagnetic spin ordered structure. But with compressive strain, the energy difference between other spin structure and FM structure get smaller because total energy is increased rapidly for FM structure compare to others. As a result, ground state is changed from ferromagnetic to G-AFM with 7 % of biaxial strain.

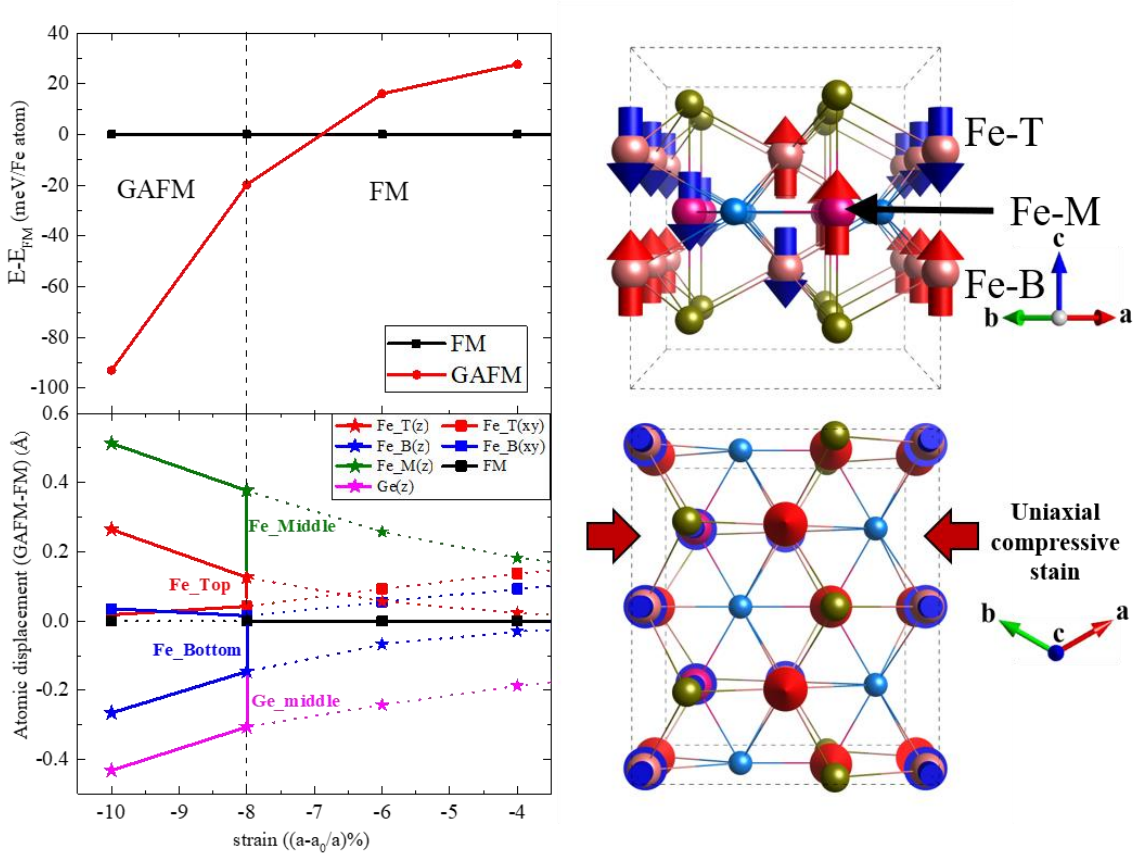

Figure 7 | Top graph : total energy difference between G-AFM spin induced structure and ferro magnetic nonpolar structure, Bottom graph : atomic displacements of each atoms as compresive strain applied.

The first graph of figure 7 shows that more clearly. Red line represents total energy of G-AFM structure compare to ferromagnetic structure depending on strain and the lines cross about 7% of strain. It means that the phase transition at 7% of strain. The next graph is atomic displacements of each atoms of FGT depending on strain. Bold lines represent displacements of ground state and dotted line means that it is not ground state displacement. Red, blue, green and magenta colors represent top iron, bottom iron, middle iron and germanium of G-AFM structure respectively. Square symbol represents in-plane displacement and star symbol represent out of plane displacement. Below the critical strain, the ground state is ferromagnetic, the displacement is zero. But above the critical strain, with phase transition from

FM to G-AFM, atomic displacement appears. If we have a look only z-directional displacement, top iron and bottom iron go up and down respectively and they may cancel most of each other's impact because they have same sign of charge. Therefore, it is close to non-polar displacement. middle iron and germanium ion go opposite direction as well, but they have opposite sign of charge, so their movements mostly contribute polarization. It makes sense that the in-plane displacement gets smaller and out of plane displacement gets larger because we applied biaxial compressive strain.

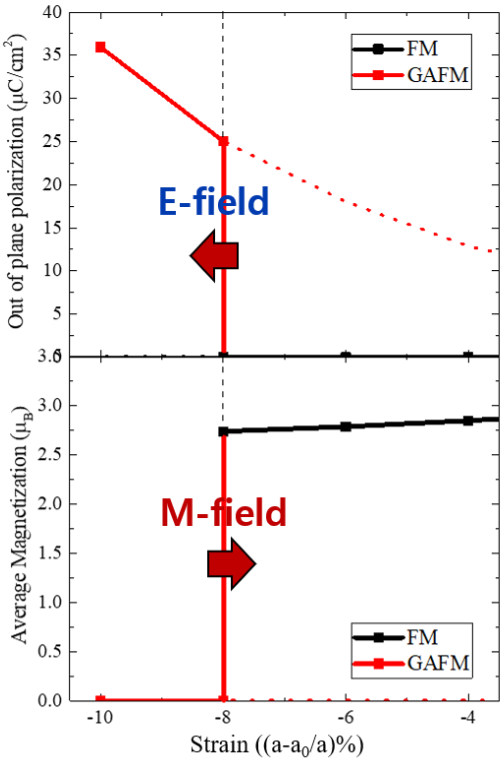

Figure 8 | Appearance of polarization and disappearance of mangnetization with phase transition from FM to G-AFM

When ferromagnetic to G-AFM phase transition occurs, the structure changes nonpolar to polar so the polar displacement and polarization appears and simultaneously magnetization goes to zero. Figure 8 shows the calculated polarization and magnetization depending on strain.

At the critical region, about 7% of compressive strain, we can expect that magnetic field would drive FGT to ferromagnetic non-polar phase and electric field would drive that to polar G-AFM phase because the energy difference between two phases are very small.

In addition, we found out that uniaxial strain stabilizes G-AFM phase more effectively. By using uniaxial strain, the critical strain goes down to only 5% of compressive strain.

The polarization here is calculated with just nominal charge. If we calculate the polarization with bon effective charge, the polarization value will be much smaller than this. I will update the data. Because FGT is metal and most of charge is screened by free electron, bon effective charge is very small. That make polarization small despite of large polar displacement.

3.4 Conclusion

In this study, the idea that symmetry breaking of simple collinear spin ordering can induce structural polar displacement in the low dimensional magnetic materials is confirmed with a practical example, FGT mono layer.

FGT is composed of strong covalent bonding between atoms. Since the energy levels of atoms are similar and there are many states that can interact with each other above and below the fermi level, it is expected that the magnetic interaction will be greatly changed by phonons. Means that spin-phonon coupling will be large. We have shown that, in materials with an odd number of magnetic layers, and with strong covalent bonds of constituent atoms, such as FGT, spin-phonon coupling results in the formation of a giant polar distortion (~0.2Å) in various antiferromagnetic meta states where translation cannot be compensated. This order is much larger than the normal spin origin polar distortion (~ 0.01Å) and even larger than the polar distortion of conventional ferroelectric materials such as $BaTiO_3$ and $BiFeO_3$. It is expected that not only FGT but also materials with strong bonding between atoms and low-dimensional characteristics of two-dimension and odd layers can exhibit a huge polar distortion due to change of magnetic state. These large polar distortions produce sizable ferroelectricity (~ 0.1 μC / cm^2) despite of the metallicity. and the meta-energy state which have polar structure produced by change of magnetic state is achieved with a uniaxial strain of about 5%.

This study not only extends the design principles that can be used to develop multiferroics, but also enable wider variety of application of multiferroics by adding degrees of freedom such as low dimension and spin[4, 26]. In addition, the formation of ferroelectrics by magnetism in low-dimensional systems will open a new chapter in the discovery and application of new states of low-dimensional materials as a general method applied to all 2-dimensional materials.

IV. Design of low dimensional multistate material

4.1 Introduction

DRAM which is the memory device widely used now already faced physical and material limitations and it is difficult to expect further improvement in performance. In addition, the need for new devices that have the advantages of high density, ultra-high speed, and ultra-low power consumption which appropriate for the forthcoming fourth revolution is more emphasized. FeRAM is one of the candidates for the new memory device[27]. FeRAM stores data 0 and 1 as up polarized state and down polarized state while DRAM store data 0 and 1 as a lack and presence of charge. Multistate material is useful for this kind of device. If the material has two different ferroelectric state, it can store double of single state device because the data can be stored as $+P_1$, $-P_1$, $+P_2$, $-P_2$ not just +P and -P. Multistate material can also be used for neuromorphic applications since neuromorphic device requires multiple inputs at once. In this context, it is important to find intrinsic multistate materials.

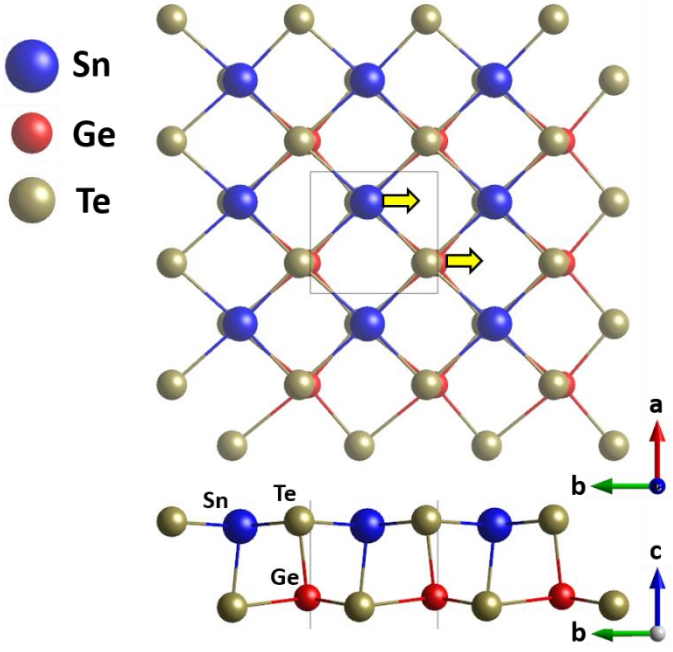

.

Figure 9 | The Simplest candidate structure of $GeSnTe_2$. Yellow arrow represent polar displacement.

Our design idea is that making multistate materials by giving structural anisotropy to the single state ferroelectric material. Many computational researches had predicted in-plane ferroelectricity and ferroelasticity of two-dimensional phosphorene analogues such as SnS, SnSe, GeS, GeSe[28, 29]. Some

previous researches even expected the possibility of room temp ferroelectricity of SnSe[30]. Not only theoretical research, in SnTe monolayer, ferroelectricity was experimentally observed with a critical temperature of 270K[5]. But for all the previous researches, the polarized state is only one since x directional and y directional polarization is not distinguishable. It because the phosphorene analogues do not have in plane structural anisotropy. To make the anisotropic structure, we mixed GeTe and SnTe which are experimentally confirmed as a ferroelectric material[5, 6]. Figure 9 shows the simplest phase of $GeSnTe_2$. For normal phosphorene analogues, the same cation located both germanium and tin sites. The yellow arrow represents polar displacement. This simple phase does not show in-plane anisotropy, but other phase gives the anisotropy and split a directional and b directional polarized state. Here we confirmed that a directional polarization and b directional polarization have different value in $GeSnTe_2$ system. Not only $GeSnTe_2$, a lot of phosphorene analogues can be a candidate. Our simple approach will contribute to boosting a wide range of multistate applications.

4.2 Computational details

First principles calculations were performed using density-functional theory (DFT) within the generalized gradient approximation GGA method with Perdew-Becke-Erzernhof parametrization as implemented in the Vienna ab initio simulation package (VASP 5.4.4). The projector augmented wave (PAW) potentials[20] explicitly include 14 valence electrons for Ge ($3d^{10}\ 4s^2\ 4p^2$), 14 for Sn ($3d^{10}\ 4s^2\ 4p^2$), 6 for Te ($5s^2\ 5p^4$). All the calculations were operated with HSE03 method and HSE calculations were carried out using the PBE potential[31-33]. A plane wave basis set with a cutoff energy of 450 eV is used. The k-point sampling uses the Monkhorst-Pack scheme[22] and employs a 6×6×1 and a 3×6×1 mesh for structure optimization of the primitive cell and the 2×1×1 supercell of $GeSnTe_2$ monolayer. The atomic positions were optimized until the interatomic forces are smaller than $1meVÅ^{-1}$. Polarization values are calculated with nominal charges, +2, +2, -4 of Ge, Sn, Te

Activation barrier for the polarization switching of $GeSnTe_2$ is was calculated by nudged elastic band method(NEB) and 3×6×1 k-point grid used for the NEB calculation[34].

4.3 Result and discussion

4.3.1 Finding ground state structure of $GeSnTe_2$

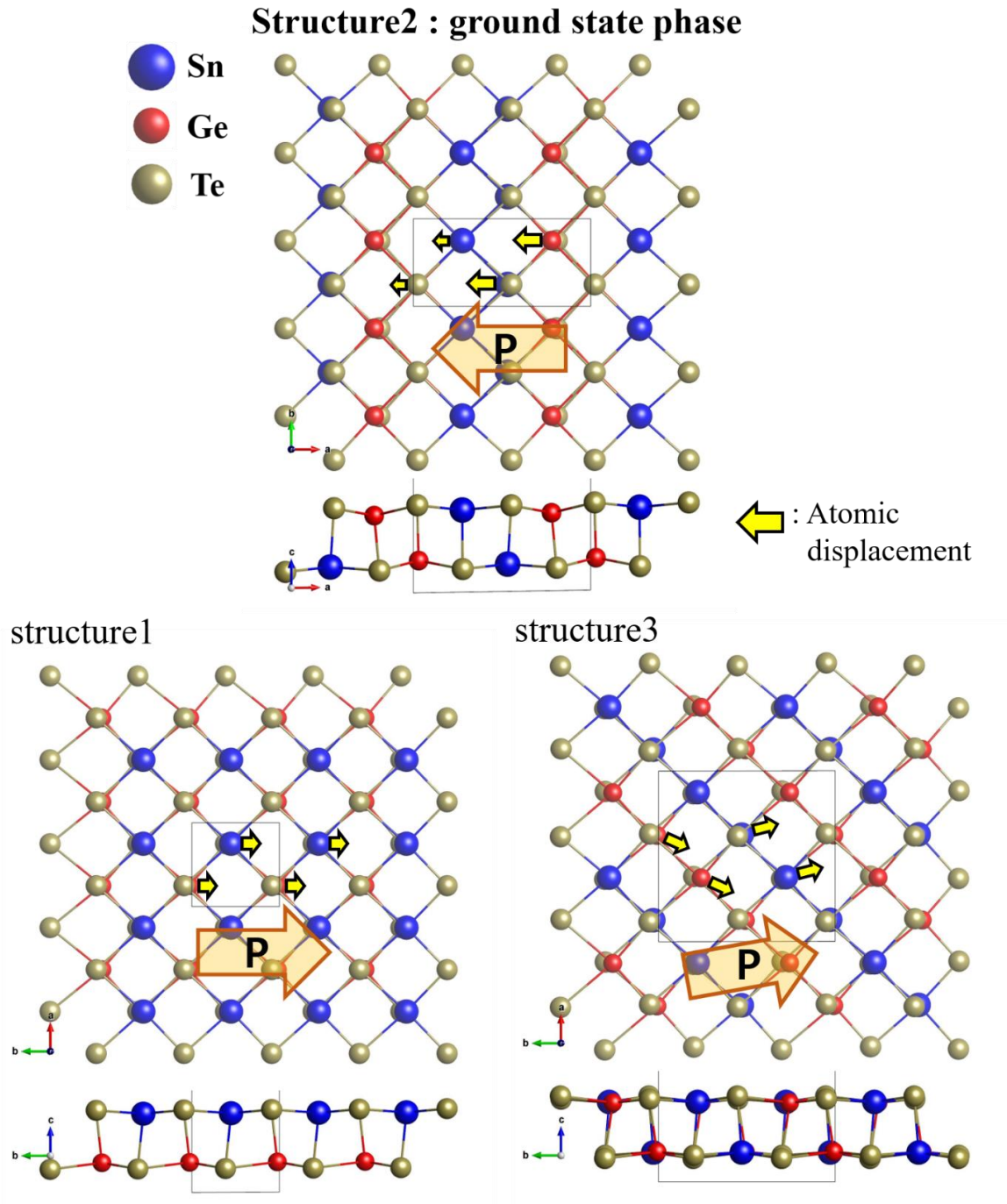

Figure 10 | The lowest energy structure that placed on the top and other different candidate structure of $GeSnTe_2$ and polar displacement patterns of each of them.

GeTe and SnTe is experimentally synthesized. Therefore, their actual structure was already analyzed. But $GeSnTe_2$ is imaginary material that haven't been experimentally synthesized yet. So, firstly, we need to find out the mixed structure of $GeSnTe_2$. To define the ground phase of $GeSnTe_2$, we made three candidate structure and compared total energy of each structure.

Figure 10 shows the ground state structure and other candidate structure. All the structures are polarized. Depending on the mixing pattern, polar displacement pattern is also changed. Among the three candidates, structure1 and structure2 has in-plane isotropic structure and only structure2 has in-lane anisotropy. Fortunately, the ground state structure was structure2 that SnTe and GeTe is alternately connected along a direction and thereby has anisotropy. The energy difference between structure1 and structure2 is 35meV/f.u. and that between structure3 and structure2 is 20meV/f.u. From this result, we can consider that mixing with keeping the original structure of SnTe and GeTe is energetically more stable.

4.3.2 Two different polarized phases of $GeSnTe_2$

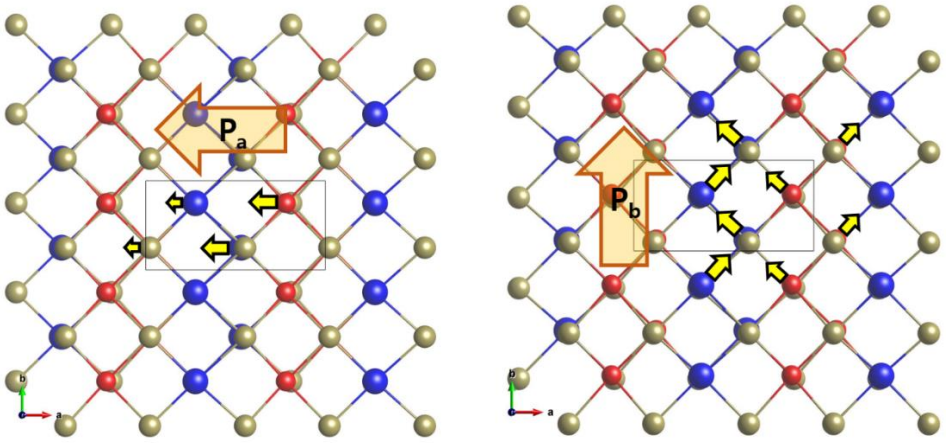

Figure 11 | a-directional and b-directional polarized phase of $GeSnTe_2$ and their polarizations.

In the previous section, we showed that the ground state phase of $GeSnTe_2$ has in-plane anisotropy. Therefore, we can expect that a-directional polarization and b-directional polarization of $GeSnTe_2$ is not the same anymore. Figure 11 shows that a-directional polarized structure of GST and b-directional polarized structure of GST. Polar displacement pattern of a-directional polar phase directly toward a direction. But that of b-directional polar phase toward diagonal direction and a component of the polarization canceled each other. The calculated polarizations are 12.434μC/cm for a direction and 13.344μC/cm^2 for b direction.

4.3.3 Energy barrier for polarization switching _NEB(nudged elastic band)

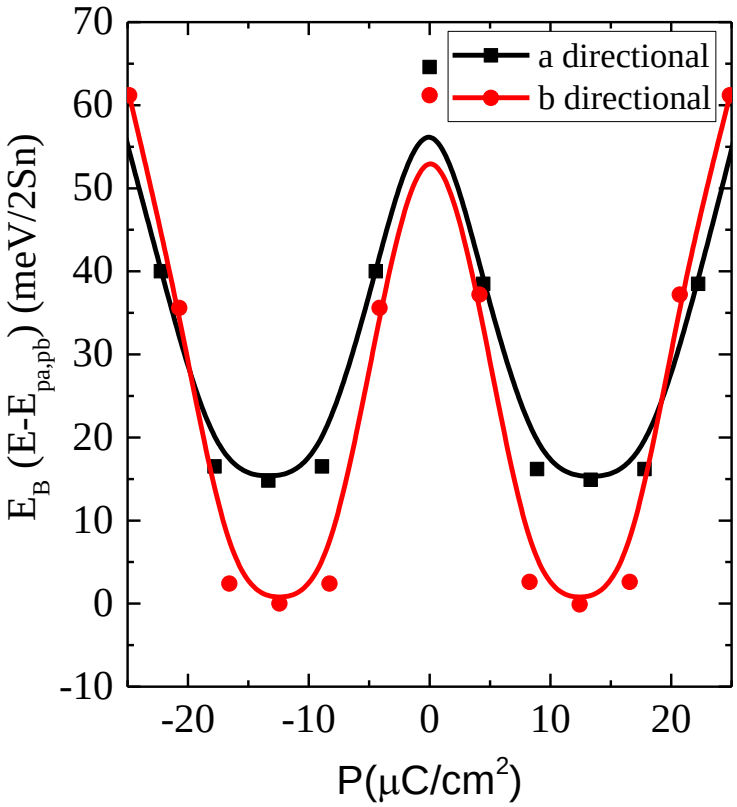

Figure 12 | Barrioer energy of direct path from -P_a,-P_b phase to +P_a,+P_b phase for polarization switching obtained from NEB calculation.

For the next, we obtained energy barrier of direct path from -P_a to P_a and -P_b to P_b through NEB calculation. The result is in the figure 12. The barrier of P_a is about 40meV/f.u. and that of P_b is about 60meV/f.u. This value is comparable to other switchable ferroelectrics. The gap between the red line minimum and black line minimum comes from total energy difference between P_a phase and P_b phase. Since P_b phase has lower energy, we must apply a directional electric field to stabilize P_a phase.

We also guessed that the polarization switching would be easier if the polar phase change from -P_b to P_a to P_b. Because the in-plane rotation can avoid a large energy destabilization of direct path. Figure 13 shows the result. The rotation path from -P_b phase to P_b phase that stop by P_a phase reduce energy barrier to 25meV/f.u. which is about half of direct path.

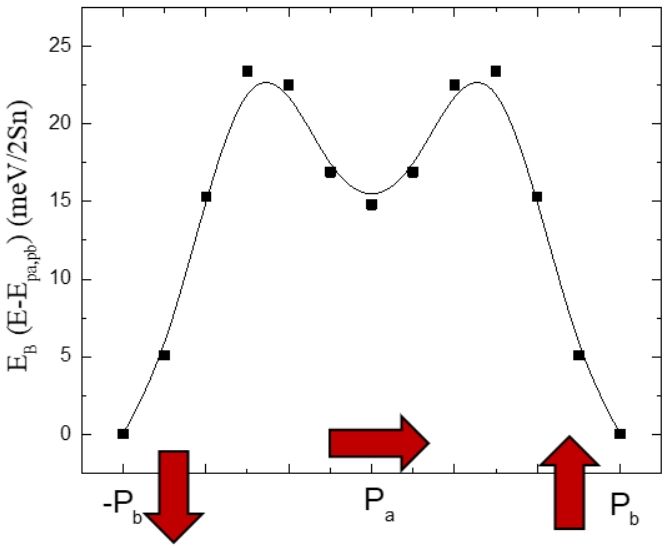

Figure 13 | Barrioer energy of rotational path from -P_b phase to +P_a phase to +P_b phase for polarization switching obtained from NEB calculation.

4.4 Conclusion

We confirmed the design idea that making multistate materials by giving structural anisotropy to the single state ferroelectric material with model system $GeSnTe_2$. To make the anisotropic structure, we mixed GeTe and SnTe which are experimentally confirmed as a ferroelectric material. Because $GeSnTe_2$ is imaginary material that haven't been experimentally synthesized, yet we made three candidate structure and compared total energy of each structure to define the ground phase of $GeSnTe_2$. From the calculation, we figured out that SnTe and GeTe is alternately connected along a-direction in the mixing structure that has lowest energy since mixing structure tend to keep the original structure of SnTe and GeTe. We assumed that the lowest energy structure as a ground state structure of $GeSnTe_2$. For this anisotropic mixing structure, a-directional polarization and b-directional polarization of $GeSnTe_2$ is not the same anymore. The calculated polarizations of the mixing structure are 12.434μC/cm for a-direction and 13.344μC/cm^2 for b-direction. Also, the barrier energies are different as well. That of P_a is about 40mev/f.u. and that of P_b is about 60meV/f.u. It means that $GeSnTe_2$ has two different polarized state. This two different polarization values and barrier energies of a-directional and b-directional polarized phase makes the multistate application possible.

V. Reference

1. Yoshinori, T.; Shinichiro, S.; Naoto, N., Multiferroics of spin origin. *Reports on Progress in Physics* **2014,** *77* (7), 076501.

2. Cohen, R. E., Origin of ferroelectricity in perovskite oxides. *Nature* **1992,** *358*, 136.

3. Wang, J.; Neaton, J. B.; Zheng, H.; Nagarajan, V.; Ogale, S. B.; Liu, B.; Viehland, D.; Vaithyanathan, V.; Schlom, D. G.; Waghmare, U. V.; Spaldin, N. A.; Rabe, K. M.; Wuttig, M.; Ramesh, R., Epitaxial BiFeO3 Multiferroic Thin Film Heterostructures. *Science* **2003,** *299* (5613), 1719.

4. Kimura, T.; Goto, T.; Shintani, H.; Ishizaka, K.; Arima, T.; Tokura, Y., Magnetic control of ferroelectric polarization. *Nature* **2003,** *426*, 55.

5. Chang, K.; Liu, J.; Lin, H.; Wang, N.; Zhao, K.; Zhang, A.; Jin, F.; Zhong, Y.; Hu, X.; Duan, W.; Zhang, Q.; Fu, L.; Xue, Q.-K.; Chen, X.; Ji, S.-H., Discovery of robust in-plane ferroelectricity in atomic-thick SnTe. *Science* **2016,** *353* (6296), 274.

6. J Polking, M.; Han, M.-G.; Yourdkhani, A.; Petkov, V.; Kisielowski, C.; Volkov, V.; Zhu, Y.; Caruntu, G.; Paul Alivisatos, A.; Ramesh, R., *Ferroelectric Order in Individual Nanometre-Scale Crystals*. 2012; Vol. 11, p 700-9.

7. Maxwell James, C., VIII. A dynamical theory of the electromagnetic field. *Philosophical Transactions of the Royal Society of London* **1865,** *155*, 459-512.

8. Borisov, P.; Hochstrat, A.; Chen, X.; Kleemann, W.; Binek, C., Magnetoelectric Switching of Exchange Bias. *Physical Review Letters* **2005,** *94* (11), 117203.

9. Kenzelmann, M.; Harris, A. B.; Jonas, S.; Broholm, C.; Schefer, J.; Kim, S. B.; Zhang, C. L.; Cheong, S. W.; Vajk, O. P.; Lynn, J. W., Magnetic Inversion Symmetry Breaking and Ferroelectricity in TbMnO3. *Physical Review Letters* **2005,** *95* (8), 087206.

10. Sergienko, I. A.; Şen, C.; Dagotto, E., Ferroelectricity in the Magnetic E-Phase of Orthorhombic Perovskites. *Physical Review Letters* **2006,** *97* (22), 227204.

11. Zhou, J. S.; Goodenough, J. B., Unusual Evolution of the Magnetic Interactions versus Structural Distortions in $R{\mathrm{MnO}}_{3}$ Perovskites. *Physical Review Letters* **2006,** *96* (24), 247202.

12. Deiseroth, H.-J.; Aleksandrov, K.; Reiner, C.; Kienle, L.; Kremer, R. K., Fe3GeTe2 and Ni3GeTe2 – Two New Layered Transition-Metal Compounds: Crystal Structures, HRTEM Investigations, and Magnetic and Electrical Properties. *European Journal of Inorganic Chemistry* **2006,** *2006* (8), 1561-1567.

13. Chen, B.; Yang, J.; Wang, H.; Imai, M.; Ohta, H.; Michioka, C.; Yoshimura, K.; Fang, M., Magnetic Properties of Layered Itinerant Electron Ferromagnet Fe3GeTe2. *Journal of the Physical Society of Japan* **2013,** *82* (12), 124711.

14. Zhuang, H. L.; Kent, P. R. C.; Hennig, R. G., Strong anisotropy and magnetostriction in the two-dimensional Stoner ferromagnet Fe3GeTe2. *Physical Review B* **2016,** *93* (13), 134407.

15. Kresse, G.; Furthmüller, J., Efficient iterative schemes for ab initio total-energy calculations using a plane-wave basis set. *Physical Review B* **1996,** *54* (16), 11169-11186.

16. Kresse, G.; Hafner, J., Ab initio molecular dynamics for liquid metals. *Physical Review B* **1993,** *47* (1), 558-561.

17. Loschen, C.; Carrasco, J.; Neyman, K. M.; Illas, F., First-principles LDA+U and GGA+U study of cerium oxides: Dependence on the effective U parameter. *Physical Review B* **2007,** *75* (3), 035115.

18. Perdew, J. P.; Burke, K.; Ernzerhof, M., Generalized Gradient Approximation Made Simple. *Physical Review Letters* **1996,** *77* (18), 3865-3868.

19. Dudarev, S. L.; Botton, G. A.; Savrasov, S. Y.; Humphreys, C. J.; Sutton, A. P., Electron-energy-loss spectra and the structural stability of nickel oxide: An LSDA+U study. *Physical Review B* **1998,** *57* (3), 1505-1509.

20. Blöchl, P. E., Projector augmented-wave method. *Physical Review B* **1994,** *50* (24), 17953-17979.

21. Kresse, G.; Joubert, D., From ultrasoft pseudopotentials to the projector augmented-wave method. *Physical Review B* **1999,** *59* (3), 1758-1775.

22. Monkhorst, H. J.; Pack, J. D., Special points for Brillouin-zone integrations. *Physical Review B* **1976,** *13* (12), 5188-5192.

23. Xiang, H.; Lee, C.; Koo, H.-J.; Gong, X.; Whangbo, M.-H., Magnetic properties and energy-mapping analysis. *Dalton Transactions* **2013,** *42* (4), 823-853.

24. Stokes, H. T.; Hatch, D. M., FINDSYM: program for identifying the space-group symmetry of a crystal. *Journal of Applied Crystallography* **2005,** *38* (1), 237-238.

25. Lee, J. H.; Fishman, R. S., Giant Spin-Driven Ferroelectric Polarization in BiFeO3 at Room Temperature. *Physical Review Letters* **2015,** *115* (20), 207203.

26. Hur, N.; Park, S.; Sharma, P. A.; Ahn, J. S.; Guha, S.; Cheong, S. W., Electric polarization reversal and memory in a multiferroic material induced by magnetic fields. *Nature* **2004,** *429*, 392.

27. de Araujo, C. A. P.; Cuchiaro, J. D.; McMillan, L. D.; Scott, M. C.; Scott, J. F., Fatigue-free ferroelectric capacitors with platinum electrodes. *Nature* **1995,** *374*, 627.

28. Hua, W.; Xiaofeng, Q., Two-dimensional multiferroics in monolayer group IV monochalcogenides. *2D Materials* **2017,** *4* (1), 015042.

29. Li, C. W.; Hong, J.; May, A. F.; Bansal, D.; Chi, S.; Hong, T.; Ehlers, G.; Delaire, O., Orbitally driven giant phonon anharmonicity in SnSe. *Nature Physics* **2015,** *11*, 1063.

30. Fei, R.; Kang, W.; Yang, L., Ferroelectricity and Phase Transitions in Monolayer Group-IV Monochalcogenides. *Physical Review Letters* **2016,** *117* (9), 097601.

31. Heyd, J.; Scuseria, G. E., Efficient hybrid density functional calculations in solids: Assessment of the Heyd–Scuseria–Ernzerhof screened Coulomb hybrid functional. *The Journal of Chemical Physics* **2004,** *121* (3), 1187-1192.

32. Heyd, J.; Scuseria, G. E.; Ernzerhof, M., Erratum: "Hybrid functionals based on a screened Coulomb potential" [J. Chem. Phys. 118, 8207 (2003)]. *The Journal of Chemical Physics* **2006,** *124* (21), 219906.

33. Heyd, J.; Scuseria, G. E.; Ernzerhof, M., Hybrid functionals based on a screened Coulomb potential. *The Journal of Chemical Physics* **2003,** *118* (18), 8207-8215.

34. Sheppard, D.; Xiao, P.; Chemelewski, W.; Johnson, D. D.; Henkelman, G., A generalized solid-state nudged elastic band method. *The Journal of Chemical Physics* **2012,** *136* (7), 074103.